

# Modelling the growth of hydrothermally synthesised bactericidal nanostructures, as a function of process conditions

Alka Jaggesar<sup>1, 2</sup> and Prasad KDV Yarlagadda<sup>1, 2\*</sup>

<sup>1</sup> School of Chemistry, Physics and Mechanical Engineering  
Science and Engineering Faculty  
Queensland University of Technology  
2 George Street, Brisbane  
Queensland 4000  
Australia

<sup>2</sup> Institute of Health and Biomedical Innovation  
Queensland University of Technology  
60 Musk Avenue, Kelvin Grove  
Queensland 4056  
Australia

\* Corresponding Author: [y.prasad@qut.edu.au](mailto:y.prasad@qut.edu.au)

**ABSTRACT** In recent times, large research focus has been placed on nanostructured materials as a method of killing bacteria. Previous work in this area has found that hydrothermally synthesised TiO<sub>2</sub> nanostructures show antibacterial behaviour against Gram-positive and Gram-negative bacteria strains. Various sources postulate that certain surface properties, such as wettability and structure dimensions are responsible for, and influence bactericidal efficiency of nanostructured surfaces. Our most recent work found that bactericidal efficiency is statistically linked to nanostructure height, leading to the demand for a method of predicting and designing nanostructure height prior to fabrication. This work uses experimental data from hydrothermal synthesis processes, in combination with IBM SPSS Statistics to form a prediction of nanostructure height, as a function of hydrothermal process parameters (NaOH concentration, reaction time and reaction temperature). Experimental validation shows that the model has a 0.5 – 8.5% error, accurately predicting the height of TiO<sub>2</sub> structures formed via hydrothermal synthesis. In addition, these samples exhibited bactericidal behaviour against both *S. aureus* and *P. aeruginosa* cells.

Keywords: Hydrothermal synthesis; bactericidal nanostructures; nanostructure growth; nanostructure height; hydrothermal model.

## 1. INTRODUCTION

Bactericidal nanotextured surfaces have risen to become a significant area of research. Studies postulate that naturally occurring micro and nanostructures found on several plant and animal species, are responsible for the inherent antibacterial and anti-biofouling affects they display [1-7]. There have been a large number of attempts to recreate these naturally occurring structures onto various metallic and polymer substrates [1, 8-16]. Common micro and nanostructure fabrication methods include hydrothermal synthesis [8, 13, 16, 17], reactive ion etching [18], nano-imprint lithography [12, 14, 19] and electron beam lithography [20-24].

There is some contention in the research community regarding the mechanism by which nanostructured surfaces kill bacteria. A biophysical model proposed by Pogodin et al (2013) suggests that nanopillar killing efficiency depends on cell membrane rigidity. This model claims that as a bacteria cell comes into contact with a nanopillared surface, regions between pillars stretch and disfigure resulting in cell rupture [2]. Further research postulates that bactericidal behaviour is dependent on the change in total free energy of the bacteria cell [25]. The presence of nanostructures on a surface increases contact adhesion area, which in turn increases the stretching degree of the cell membrane, ultimately causing rupture and death.

In contrast, Xue et al (2015) proposed that the killing mechanism occurs at the top of the nanopillar ridge, where maximum stretching of the membrane occurs [26]. This was supported by Velic et al (2019), who used finite element modelling techniques to model the interaction between *B. subtilis* and nanopillars. This work suggests that local deformation stresses to the peptidoglycan layer occur at the tip of the pillar, causing rupture [27]. An additional finding from this work is that the aspect ratio (ratio of diameter to height) of the nanopillars influences bactericidal efficiency. Therefore, bacterial adhesion to a surface is a multi-faceted and complex issue, which depends on several factors such as structure aspect ratio, surface wettability, initial physical attraction to the surface and other physical, biological and chemical processes. It is a combination of these aspects that determines adhesive and cohesive properties of the biofilm.

Researchers believe there are a number of surface properties that influence bactericidal efficiency, such as wettability [1, 9, 28-30] and structure height, diameter and density [27, 31]. In our previous work, bactericidal efficiency of hydrothermally nanostructured TiO<sub>2</sub> against both Gram-negative and

Gram-positive bacteria was statistically correlated to nanostructure height [32]. From this finding, it became important to understand and predict the growth of nanostructures during hydrothermal synthesis, given specified experimental conditions.

Hydrothermal synthesis is a very commonly used method for fabricating nanotextured surfaces due to its reliability, environmentally friendly nature, simplicity, low cost compared to other methods, and flexibility for material morphology control [13, 17]. During the heterogeneous reaction, high temperature and pressure dissolve and recrystallise the material in a vessel [33, 34]. The process is effective at producing various morphologies, such as nanoparticles, nanorods, nanowires and nanotubes. Adjusting precursor concentration, solvent composition, solvent pH, operation temperature and reaction duration, alters nanoparticle shape, size and surface roughness [34-37]. For example, high hydrothermal precursor concentration generally affects morphology and increases density (forming closely packed arrays) and diameter of fabricated structures [38]. Similarly, longer hydrothermal reaction time produces larger particles [33, 39], with the same effects seen with reaction temperatures above 180°C. These parameters have also been found to affect the crystalline properties of the material [40]. While these phenomena have been qualitatively observed over the years, quantitative modelling of the behaviour is lacking.

Currently, modelling relating to the hydrothermal process is limited to thermodynamic and kinetic modelling, in the form of phase stability and yield diagrams, which allow control over chemical phases in the reaction and product. These models use Gibb's energies, enthalpies, and entropies at specified reference temperatures [41] to give equilibrium concentrations of all species involved in the reaction as a function of pH, temperature and initial concentrations. Diagrams show the range of equilibrium conditions for stable aqueous and solid products in the hydrothermal reaction. Yield diagrams provide a theoretical product yield at specified conditions, and assist in indicating the range of reaction conditions which result in the desired ceramic phase [41, 42]. The original model was proposed by Lencka et al (1993), and was developed and verified using barium titanate ( $\text{BaTiO}_3$ ) and lead titanate ( $\text{PbTiO}_3$ ), resulting in stability diagrams for both Ba-Ti and Pa-Ti [43]. This idea has been expanded to generate yield diagrams for  $\text{BaWO}_4$  [44] and  $\text{PbTiO}_3$  with a tetramethylammonium hydroxide mineralizer [45]. More recently, thermodynamic yield models for the synthesis of nickel tungstate, as a function of temperature, pH and reagent reaction were developed [46].

While these diagrams and models are useful, they are applicable to hydrothermal synthesis of ceramic powders [41], and cannot be applied to nanostructures grown on metallic substrates. While the effect of various hydrothermal process parameters has been extensively experimentally and qualitatively investigated, this has not been quantitatively reported. Thus far, researchers have not yet developed a model to describe the height of hydrothermally synthesised structures using solid metallic substrates, as a function of hydrothermal conditions. Therefore, this work develops a relationship between nanostructure height as a function of NaOH concentration, reaction temperature and reaction duration using a statistical modelling approach. A quantitative representation of hydrothermal growth is an important aspect and contribution to the hydrothermal process, to improve process efficiency and predict resulting material properties prior to fabrication.

## 2. MATERIAL AND METHODS

This section outlines the materials and methods used to fabricate, measure, model and validate  $\text{TiO}_2$  nanostructure growth, and bacterial viability testing.

## 2.1 Experimental design

Nanotextured TiO<sub>2</sub> surfaces were fabricated using hydrothermal synthesis. Hydrothermal conditions (NaOH concentration, reaction time and reaction temperature) were altered to produce a wide range of surface textures and TiO<sub>2</sub> structure heights. NaOH concentration ranged from 0.1 – 2.0 M, reaction time from 1 – 10 hours and reaction temperature from 120 – 240°C. These parameter value ranges were selected for several reasons. Firstly, the reaction temperature value range was influenced by process constraints, where hydrothermal structures have been found to only grow above 100°C [33] and the hydrothermal vessel cannot exceed 240°C, as per manufacturer and safety instructions. Reaction time and NaOH concentration ranges were selected after trial and error processes.

Factorial experimental design was selected for the fabrication experiments, to ensure a robust statistical model. Table 1 shows hydrothermal fabrication conditions used to develop the model. Three samples were fabricated for each hydrothermal condition listed in Table 1.

Table 1: Hydrothermal conditions tested

Sample Name (Conc(M)_Time (Hrs)_Temp(°C))	NaOH Concentration (M)	Reaction Time (Hrs)	Reaction Temperature (°C)
0.1_3_240	0.1	3	240
0.25_3_240	0.25	3	240
0.5_3_240	0.5	3	240
1.0_3_240	1.0	3	240
1.5_3_240	1.5	3	240
2.0_3_240	2.0	3	240
1.0_3_120	1.0	3	120
1.0_3_145	1.0	3	145
1.0_3_170	1.0	3	170
1.0_3_195	1.0	3	195
1.0_3_220	1.0	3	220
1.0_1_240	1.0	1	240
1.0_2_240	1.0	2	240
1.0_5_240	1.0	5	240
1.0_8_240	1.0	8	240
1.0_10_240	1.0	10	240
0.5_3_120	0.5	3	120
0.5_3_170	0.5	3	170
2.0_3_120	2.0	3	120
2.0_3_170	2.0	3	170
0.1_3_120	0.1	3	120

<i>0.1_3_170</i>	0.1	3	170
<i>0.1_1_240</i>	0.1	1	240
<i>0.1_10_240</i>	0.1	10	240
<i>2.0_1_240</i>	2.0	1	240
<i>2.0_10_240</i>	2.0	10	240
<i>1.0_1_120</i>	1.0	1	120
<i>1.0_10_120</i>	1.0	10	120
<i>1.0_1_170</i>	1.0	1	170
<i>1.0_10_170</i>	1.0	10	170
<i>0.1_1_120</i>	0.1	1	120
<i>2.0_1_120</i>	2.0	1	120
<i>0.1_10_120</i>	0.1	10	120
<i>2.0_10_120</i>	2.0	10	120
<i>0.1_1_170</i>	0.1	1	170
<i>2.0_1_170</i>	2.0	1	170
<i>0.1_10_170</i>	0.1	10	170
<i>2.0_10_170</i>	2.0	10	170

## *2.2 Nanotexture surface fabrication*

Hydrothermal synthesis was used to fabricate TiO<sub>2</sub> micro and nanostructures on titanium substrates. 1 cm<sup>2</sup> titanium plates were polished to a 0.04 μm surface roughness. Plates were sonicated in acetone for 10 minutes, rinsed 3 times with 18.2 MΩ H<sub>2</sub>O, and dried with N<sub>2</sub> gas. Samples were then placed in a custom-made PTFE holder in a 125 mL Parr acid digestion vessel, with 60 mL NaOH. Various concentrations of the NaOH solution were tested, as presented in Table 1. The sealed digestion vessel was placed in the oven, and heated to the specified reaction temperature. Reaction time was measured from the time temperature had stabilised. After the given reaction time, samples were removed from the oven and completely cooled. Samples were then removed from the vessel, rinsed 3 times in 18.2 MΩ H<sub>2</sub>O and dried with N<sub>2</sub> gas. Samples were placed into a furnace and annealed for 1 hour at 300°C (10°C/min heating rate), and removed when the furnace had cooled below 80°C. Once at room temperature, samples were submerged in 20 mL of 0.6 M HCl solution for 30 minutes. Samples were once again rinsed 3 times in 18.2 MΩ H<sub>2</sub>O and dried with N<sub>2</sub> gas. Finally, samples were calcined in the furnace for 2 hours at 600°C (10°C/min heating rate) and left to cool in the furnace until the furnace temperature reached 80°C.

## *2.3 Structure height measurements*

Three samples were fabricated for each hydrothermal condition shown in Table 1. The JEOL JSM-7001F SEM was used to measure the structure height of 10 randomly selected structures from each sample, giving a total of 30 structure height measurements per hydrothermal condition. Samples were tilted to ensure the substrate surface was seen, ensuring accurate measurement. Structure height measured using in-built JEOL software which took into account tilt angle a trigonometric calculations.

“Structure height” is defined as the length of the structure from the substrate surface to the structure tip (excluding substrate thickness).

#### 2.4 Statistical modelling

A statistical modelling approach was adopted for this study, due to the nature of the data collected and the highly complex nature of the corrosion and crystallization process that occurs during a hydrothermal reaction. The statistical model was developed in IBM SPSS Statistics by first creating a database of all experimental conditions and associated height measurements (30 measurements per experimental condition). Values for nanostructure height, NaOH concentration, reaction time and reaction temperature were normalised by dividing each measured value by the lowest recorded value in the study. Descriptive statistics (scatterplots, means, medians and data normality) was used to investigate the nature of data. Univariate regression was then completed for all experimental conditions to develop the relationship between height and each individual normalised parameter (NaOH concentration ( $C^*$ ), reaction time ( $t^*$ ) and reaction temperature ( $T^*$ ). Initially, all parameters from 1 to 3 orders were included in the regression (e.g.  $C$ ,  $C^2$  and  $C^3$ , etc.) and insignificant terms ( $p > 0.05$ ) were removed to improve model accuracy. The statistical model gives the normalised nanostructure height, as a function of normalised NaOH concentration, temperature and time ( $f(h^*) = C^*, T^*, t^*$ ). Qualitative validation was completed by analysing normality, P-P and Q-Q curves of the model. In addition, quantitative statistical data from the model, such as skewness and kurtosis were examined for model accuracy.

#### 2.5 Experimental model validation

To validate the statistical model, three sets of hydrothermal conditions were experimentally tested, and resulting nanostructure heights measured. Experimental conditions used for model validation were not previously used in development and building the model itself, but lie within the same ranges for NaOH concentration (0.1 – 2.0 M NaOH), reaction time (1 – 10 hours) and reaction temperature (120 – 240°C). Validation of the model is highly important, as it indicates the accuracy of the model when applied to data sets other than the ones used to develop it. The aim of validating the model is to obtain a maximum of 15% error between the predicted nanostructure height and the measured average structure height. The following hydrothermal conditions (Table 2) were used for experimental validation.

Table 2: Hydrothermal conditions for statistical model validation samples

Sample Name (Conc(M)_Time (Hrs)_Temp(°C))	NaOH Concentration (M)	Reaction Time (Hrs)	Reaction Temperature (°C)
0.3_1.5_130	0.3	1.5	130
0.8_6.5_180	0.8	6.5	180
1.8_9_230	1.8	9	230

For experimental validation of the model, 3 samples for each hydrothermal condition from Table 2 were fabricated, with 10 measurements for structure height taken from each sample using the JEOL7000F SEM, giving a total of 30 height measurements per hydrothermal condition.

To find the theoretical prediction for the average structure height, values for NaOH concentration, reaction time and reaction temperature for each sample were entered into the prediction model and  $h$  calculated. Percentage error (%) was calculated using:

$$\text{Percentage Error (\%)} = ((\text{Predicted Value} - \text{Measured Value}) / \text{Measured Value}) \times 100$$

### 2.6 Bacterial testing

The model validation hydrothermal samples were also tested for their bactericidal behaviour. The viability of Gram-positive *S. aureus* (ATCC 25923) and Gram-negative *P. aeruginosa* (ATCC 27853) was tested using the plate-count method. Bacteria cells were suspended in 5 mL sterile nutrient broth and left to grow to an OD<sub>600</sub> of 0.3. The suspension was diluted using PBS, adjusting OD<sub>600</sub> to 0.1. The re-suspended cells were diluted (1:10 with PBS) and incubated at 37°C in triplicate with the nanostructured sample. Both a flat Ti-6Al-4V sample, and a well of bacteria suspension alone (without substrate material, to measure the natural growth and death of the bacteria with time) were used as control samples. 100 µL of each suspension was sampled, appropriately diluted, spread on nutrient agar plates and incubated for 18 hours at 37°C (suspensions were sampled at 0, 3 and 18-hour time points). Agar plates were imaged using GeneSnap software and colonies counted using ImageJ. Colony forming units (CFU) per mL were calculated for each surface and an average value found.

The suspension was removed from the well plates at the end of the test, and bacteria were fixed using 3% glutaraldehyde (C<sub>5</sub>H<sub>8</sub>O<sub>2</sub>). Samples were then washed twice in PBS and stored in PBS overnight. Samples were fixed by washing in 0.1 M cacodylate buffer, 1% OsT<sub>4</sub>, and then dehydrated using an ethanol series (50, 70, 90 and 100%) and hexamethyldisiloxane (C<sub>6</sub>H<sub>19</sub>NSi<sub>2</sub>). Samples were gold coated using a Leica EM SCD005 sputter coater for 75 seconds and imaged under SEM. Bacteria tests were repeated to confirm results, for both bacteria strains.

## 3. RESULTS

This section describes fabrication and measurement results of the structured surfaces and presents the model and validation for predicting nanostructure height. Results of bacterial viability tests performed on validation samples are also presented.

### 3.1 Surface morphology with changes in process parameters

SEM images of fabricated samples are shown in the Supplementary Information provided. These images show that in general, process parameters (NaOH concentration, reaction time and reaction temperature) play a critical role in the shape, dimension and general morphology of hydrothermally synthesised structures. Supplementary Information Figure 1 shows that NaOH concentration has a profound effect on general surface morphology. The figure shows that as NaOH concentration increases, surface morphology changes from small random nanostructures (Supplementary Figure 1a and b), to longer pillar-like structures (Supplementary Figure 1c and d), and finally to large, interconnected mesh-like structures at high NaOH concentrations (Supplementary Figure 1e and f). The most significant change in morphology occurs between 1.0 and 1.5 M NaOH, where structures change from pillars to a mesh-like array. This change in structure has an associated increase in array height (Table 3), where structure height increases from 307 nm (at 1.0 M) to 881 nm (at 1.5 M).

When varying hydrothermal reaction temperature (with constant reaction time (3 Hrs) and NaOH concentration (1.0 M NaOH)), results show a conservative effect on surface morphology (Supplementary Figure 2). At 120°C structures appear to be connected at the pillar tips, which separate

as temperature increases, becoming individualised. The change in morphology is less pronounced compared to morphology changes with NaOH concentration.

The effect of reaction time on surface morphology is interesting. Supplementary Figure 3 shows surface morphology with increasing reaction time (1 – 10 Hrs), at constant NaOH concentration (1.0 M) and reaction temperature (240°C). As time increases, structures grow from individualised pillar-like structures (Supplementary Figure 3a – c) to mesh-like arrays (Supplementary Figure 3d – f). There is a general increase of structure height with hydrothermal reaction time, with a sharp increase in height between 3 and 5 hours. During this time, structures grow from nanoscale to microscale structures, with the largest array formed at 8 hours of reaction. After this time, the average structure height decreases (Table 3). Supplementary Figures 4 – 8 show SEM images of hydrothermal surface production when varying multiple parameters simultaneously. These SEM images cannot be analysed for morphological changes, due to the simultaneous alteration of the parameters. However, the results of these experiments (i.e. structure dimensions) were used to develop the statistical model.

### 3.2 Prediction model

TiO<sub>2</sub> structured surfaces were fabricated and measured using hydrothermal synthesis and SEM software, as described. 3 samples were fabricated for each experimental condition (Table 1), with 10 measurements for height taken from each sample, giving 30 height measurements per experimental condition. These 30 measurements were used in developing the prediction model in IBM SPSS Statistics, however the average height for each hydrothermal condition is shown in Table 3, as well as the average normalised height for each sample, found by the following equation:

$$h^* = h \text{ (nm)} / 28.1 \text{ (nm)}$$

Where  $h^*$  is the normalised height,  $h$  is the measured height and 28.2 nm is the smallest height value measured in the data set.

Table 3: Average height and normalised height

Sample Name	Average Height (nm)	Average Normalised Height
1.0_3_240	306.5	10.9
0.5_3_240	302.0	10.8
1.5_3_240	881.3	31.4
2.0_3_240	1316.7	46.9
0.1_3_240	188.4	6.4
0.25_3_240	210.5	7.4
1.0_3_120	328.4	11.7
1.0_3_145	260.2	9.3
1.0_3_170	336.0	11.9
1.0_3_195	467.7	16.6
1.0_3_220	449.8	16.0
1.0_1_240	244.2	8.7

<i>1.0_2_240</i>	416.3	14.8
<i>1.0_5_240</i>	5926.7	210.9
<i>1.0_8_240</i>	7337.3	261.1
<i>1.0_10_240</i>	6884.3	245.0
<i>0.5_3_120</i>	192.7	6.9
<i>0.5_3_170</i>	216.4	7.7
<i>2.0_3_120</i>	527.4	18.8
<i>2.0_3_170</i>	520.7	18.5
<i>0.1_3_120</i>	46.6	1.7
<i>0.1_3_170</i>	188.2	6.7
<i>0.1_1_240</i>	95.5	3.4
<i>0.1_10_240</i>	103.8	3.7
<i>2.0_1_240</i>	229.9	8.1
<i>2.0_10_240</i>	14769.7	526.6
<i>1.0_1_120</i>	272.5	9.7
<i>1.0_10_120</i>	488.7	17.4
<i>1.0_1_170</i>	841.0	29.9
<i>1.0_10_170</i>	852.9	30.4
<i>0.1_1_120</i>	79.7	2.8
<i>2.0_1_120</i>	299.1	10.6
<i>0.1_10_120</i>	253.8	9.0
<i>2.0_10_120</i>	654.3	23.3
<i>0.1_1_170</i>	53.8	1.9
<i>2.0_1_170</i>	452.8	16.1
<i>0.1_10_170</i>	234.1	8.3
<i>2.0_10_170</i>	1091.0	38.8

When developing the prediction model all parameters were initially included. Statistically non-significant ( $p > 0.05$ ) parameters were then removed, improving the  $R^2$  value and generalisability. Parameter estimates and associated significance for each term in the model is shown in Table 4.

*Table 4: Parameter estimates for prediction model*

Parameter	B	Std. Error	Sig.
-----------	---	------------	------

Time <sup>3</sup>	-0.029	0.002	0.000
Time <sup>2</sup>	0.401	0.023	0.000
Time	-1.026	0.085	0.000
Temperature	0.751	0.046	0.000
Concentration <sup>2</sup>	-0.007	0.000	0.000
Concentration	0.246	0.010	0.000
Intercept	0.143	0.136	0.000

The table shows that all parameters included in the model are highly statistically significant, with the highest order occurring for the time parameter (3<sup>rd</sup> order polynomial). Interestingly, NaOH concentration reached 2 orders, and reaction temperature only 1. Combining these parameter coefficient estimates into 1 equation gives the following expression:

$$\ln(h^*) = -0.029t^{*3} + 0.401t^{*2} - 1.026t^* - 0.007C^{*2} + 0.246C^* + 0.751T^* + 0.143$$

Where  $h^*$  is normalised structure height,  $C^*$  is normalised NaOH concentration,  $T^*$  is normalised reaction temperature and  $t^*$  is normalised reaction time, calculated using the following equations:

$$C^* = C (M)/0.1 (M)$$

$$t^* = t (Hr)/1 (Hr)$$

$$T^* = T (^{\circ}C)/120 (^{\circ}C)$$

The prediction model has an adjusted R<sup>2</sup> value of 0.775, showing a good fit to the data. Figure 1 and Table 5 show the residual data for the model, highlighting the model's statistical validity. Firstly, the scatterplot of the standardised residual values vs. the model's predicted values (Figure 1a) shows a large number of randomly placed residuals, which is a positive outcome, indicating that the model fits the data well.

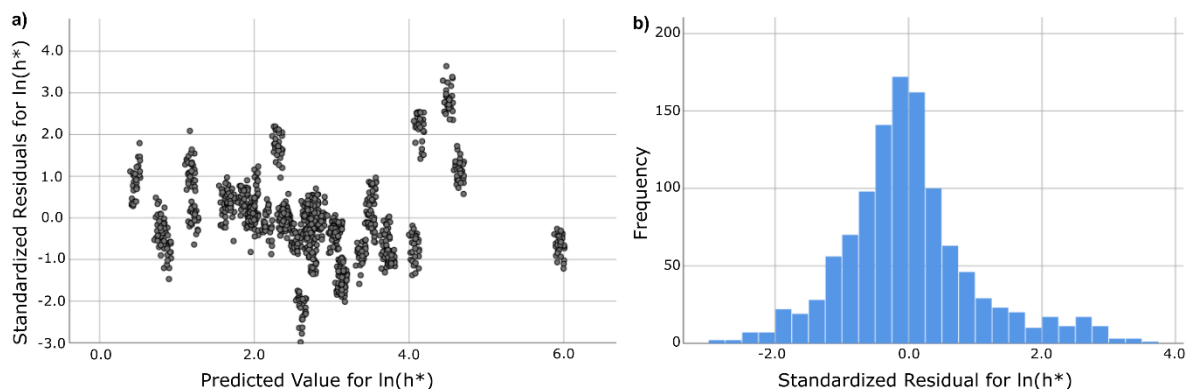


Figure 1: a) residual data for prediction model b) normality plot of residual data

Secondly, the normality plot of the residual data (Figure 1b) shows a very clear bell curve, indicating a high level of normality for the residual values. In addition, the residual descriptive data (Table 5) shows that the mean (0.000) and median (-0.0844) values for the standardised residuals are similar in value.

Furthermore, the kurtosis (1.255) and skewness values (0.647) are within the acceptable ranges ( $\pm 3.0$ ).

Table 5: Standardized residual descriptive statistics for  $\ln(h^*)$

Descriptive	Statistic	Std. Error
Mean	0.0000	0.02940
Median	-0.844	
Variance	0.985	
Skewness	0.647	0.072
Kurtosis	1.255	0.145

To further validate this model, P-P and Q-Q plots were created in SPSS (Figure 2). The P-P plot (Figure 2a) compares the observed cumulative distribution function of the standardised residuals to the optimal normal distribution (indicated by the linear line from (0, 0) to (1, 1)). The plot shows that the standardised residuals are consistent and close to the desired normality function, supporting the model's validity. Similarly, the Q-Q plot (Figure 2b) compares the observed quantile (also known as percentiles) with the theoretical quantile of the normal distribution. The majority of this function matches the normal distribution well, however at various points there is some deflection away from the normal distribution line, which is reflected in the adjusted  $R^2$  value (0.775). This indicates that the data has several more extreme values than would be expected if they truly came from a normal distribution.

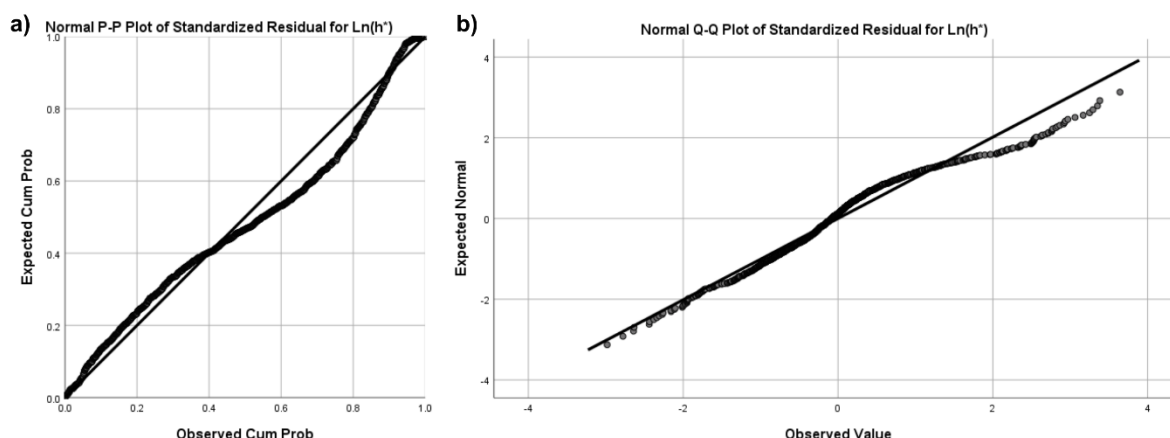


Figure 2: a) P-P plot and b) Q-Q plot of residual data values for prediction model

From the analysis of the adjusted  $R^2$  value, residual data, Q-Q and P-P plots, the model is statistically valid and acceptable. As this model includes all three parameters (NaOH concentration, reaction time and reaction temperature) at statistically significant levels, it can be said that these three hydrothermal parameters play key roles in the growth of nanostructures. This prediction model quantifies the effect of each parameter within the range of conditions tested.

### 3.3 Experimental validation

The model developed above gives a theoretical approximation for the average height of structures formed during hydrothermal reaction between Ti and NaOH (within the mentioned parameter bounds). Whilst this model is statistically valid, experimental validation was used to further strengthen

the validity of this model, using different conditions (Table 2) for NaOH concentration, reaction time and reaction temperature, than those used to form the prediction model.

Validation samples were fabricated and measured using the hydrothermal process described. Figure 3 shows SEM images of the three validation samples. From these images it can be seen that the size of the structures increases as NaOH concentration, time and temperature increase. Small TiO<sub>2</sub> bumps are formed at conservative conditions (sample 0.3\_1.5\_130, Figure 3a). Conditions of 0.8 M NaOH reacted for 6.5 hrs at 180°C has given a multilayer structure morphology, showing a combination of small sharp structures and large flake-like structures (Figure 3b). The largest structures were formed at high NaOH concentration (1.8 M), temperature (230°C) and time (9 hrs) conditions (Figure 3c).

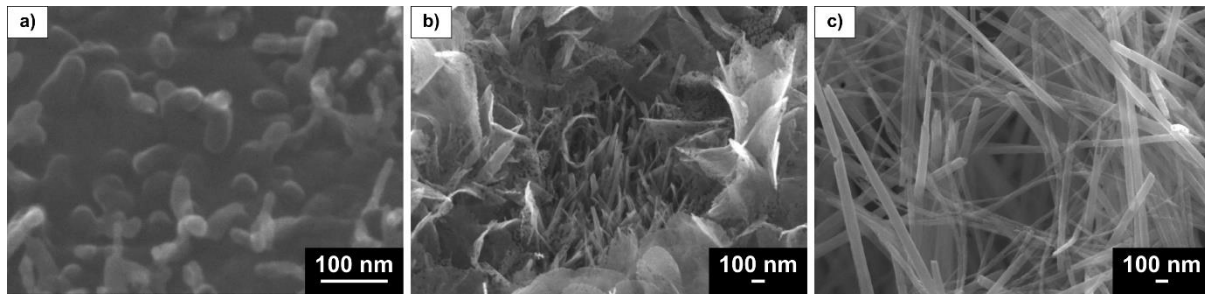


Figure 3: SEM image of a) 0.3\_1.5\_130, b) 0.8\_6.5\_180 and c) 1.8\_9\_230

Table 6 shows the average predicted height (using the prediction model) and measured average height (average of 30 height measurements per sample).

Table 6: Experimental validation of hydrothermal height prediction model

Sample Name	Predicted Height (nm)	Measured Height (nm)	Percentage Error (%)
0.3_1.5_130	68.90	64.08 ± 1.18	7.0
0.8_6.5_180	4602.68	4209.67 ± 50.9	8.5
1.8_9_230	9741.85	9697.25 ± 1160	0.5

The table shows that the measured heights of the validation structures are similar to values obtained using the prediction model. Sample 0.3\_1.5\_130 had a predicted structure height of 68.90 nm, and a measured mean height of 64.08 nm (an approximate 7% difference). Structures formed at moderate hydrothermal conditions (0.8 M, 6.5 hrs and 180°C) had an 8.5% difference to the predicted height.

Similarly, sample 1.8\_9\_230 had a predicted average structure height of 9742 nm, with a measured mean structure height of 9697 nm (difference of 0.5%). This is a very favourable result, showing that the model is a good estimate for predicting the average structure height of hydrothermally synthesised textured surfaces.

### 3.4 Bacteria viability testing

Bacteria viability of *S. aureus* and *P. aeruginosa* was tested on the three validation surfaces, to ensure bactericidal properties. Figure 4 shows the CFU/mL of *S. aureus* and *P. aeruginosa* as a percentage of the control sample (cell suspension with no substrate material). Flat, polished Ti-6Al-4V was also used to compare flat surfaces to hydrothermally synthesised textured surfaces. Statistically significant results are indicated.

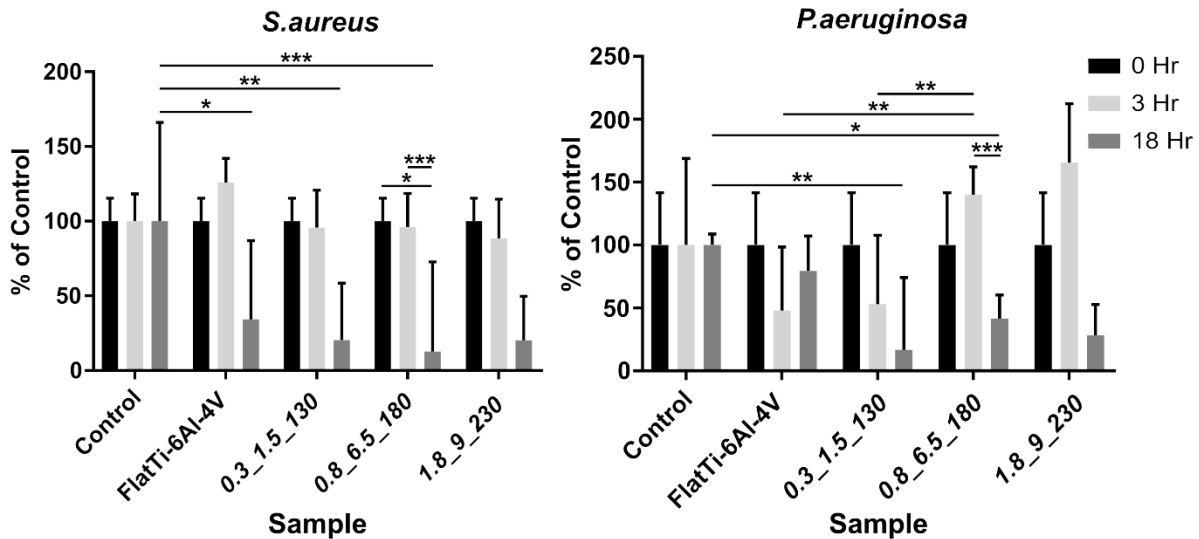


Figure 4: Bactericidal efficiency of extended study samples against *S. aureus* and *P. aeruginosa*, \* $p < 0.1$ , \*\* $p < 0.01$ , and \*\*\* $p < 0.001$

Results show that *S. aureus* CFU/mL decreased from 0 – 3 hours for all samples, which is followed by a substantial reduction between 3 – 18 hours for all nanostructured samples. These are encouraging results, given that the flat Ti-6Al-4V surface has increased in CFU/mL between 0 – 3 hours. The results show that after 18 hours of incubation, the flat material and three nanotextured surfaces have greatly reduced the number of *S. aureus* colonies, with the three textured surfaces causing the greatest cell death. The three validation surfaces produced relatively similar bactericidal efficiency, with sample 0.8\_6.5\_180 (average height 4603 nm) showing a marginally higher efficiency than samples 0.3\_1.5\_130 and 1.8\_9\_230.

The results of the *P. aeruginosa* viability test shows that after 18 hours of incubation, textured surfaces (validation sample surfaces) show the greatest cell death, with sample 0.3\_1.5\_130 (average height  $64.08 \pm 1.18$  nm) producing the highest bacteria death. As with the *S. aureus* test, the CFU/mL of *P. aeruginosa* cells show a large difference between 3 and 18 hours, indicating that the structures have the greatest bactericidal impact between these time points. A reason for this is that by this time cells have passed their initial high division rate and have achieved steady growth. At this stage, the bactericidal efficiency of the textured surface (and therefore rate of cell death) is higher than the cell growth rate, thus reducing the overall CFU/mL of the bacteria.

Figure 5 shows SEM images of *S. aureus* and *P. aeruginosa* bacteria on the validation sample surfaces. From these images, piercing and spreading of bacteria is clearly seen. The collapse of *P. aeruginosa* bacteria is especially prevalent on the 0.8\_6.5\_180 surface (Figure 5d), where complete cell collapse and deformation can be observed on the TiO<sub>2</sub> flake structure. The images show that the large array height of the 1.8\_9\_230 samples (Figure 5e and f) are effective at piecing both bacteria types. The images show that the 0.3\_1.5\_130 sample (Figure 5a and b) does not have this piecing effect, due to the small structure size and low aspect ratio, and is therefore less effective at killing bacteria.

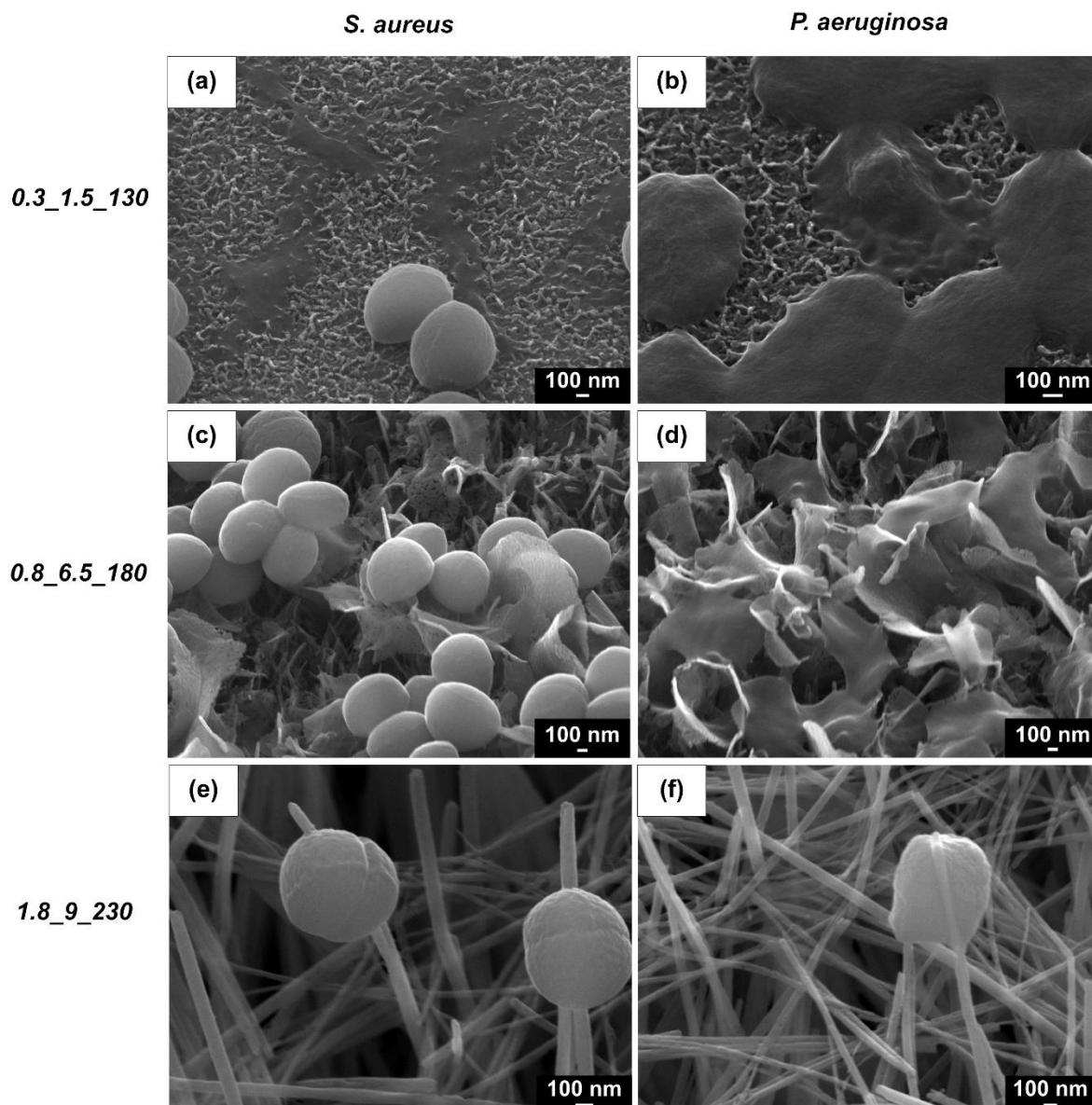


Figure 5: SEM images of *S. aureus* (a, c and e) and *P. aeruginosa* (b, d and f) on validation sample surfaces

#### 4. DISCUSSION

The prediction model developed in this work sheds light into the mechanisms and parameters that affect hydrothermal synthesis and nanostructure growth. The model developed shows NaOH concentration, reaction temperature and reaction time play key roles in structure growth, however their degree of impact appears to be unequal. By examining samples formed in all experimental conditions in this study, as well as the parameter estimates and order of each parameter, there are several physical implications that can be deduced. Increasing NaOH concentration leads to the formation of highly dense, close-packed mesh-like structures due to the increased number of nucleation sites at higher NaOH concentrations. As structures grow they fuse together with neighbouring structures [16, 39], thereby creating the highly connected arrays observed. Reaction temperature has a large impact on the structure height and length, and reaction time largely influences the array height and nanostructure diameter.

Table 6 shows that the larger the predicted (and measured) nanostructure height, the larger the associated standard error. This indicates that larger arrays have a larger range in structure height, compared to smaller structures. At low hydrothermal conditions, structure height is more controlled and consistent, giving smaller associated measurement error. At more extreme reaction conditions, and particularly when structures combine to form a mesh-like array, there is a much larger range in structure height.

Error between the predicted height given by the model and measured height is expected, given that the hydrothermal process is a chemical reaction. While every effort was made to ensure consistency throughout experimentation, it is likely that some factors may have caused fluctuations in resulting surface properties. These include considerations such as vessel pressure, rate of vessel cooling (dependent on ambient temperature), and difference in chemical batches (e.g. acetone and NaOH). In addition, SEM images and recorded height measurements for each condition show variation in structure heights over the substrate surface. These structures do not have a uniform and consistent spacing, density, diameter and heights, due to the nature of the hydrothermal process. These reasons, combined with the inherent nature of chemical reactions, make predicting the nanostructure height without error an unrealistic notion.

Through the various forms of validation used in this study and given the unpredictable and random nature of chemical reactions, this model provides a sound basis for determining the approximate height of hydrothermally fabricated TiO<sub>2</sub> nanostructures. The favourable residual statistics, adjusted R<sup>2</sup> value and the validation experiments show that the proposed model is an accurate representation of structure height. The model can be used for predicting the array height of TiO<sub>2</sub> structures formed using hydrothermal fabrication, and is functional between 0.1 to 2.0 M NaOH, 120 and 240°C and 1 and 10 hours.

Bacteria viability tests show that the samples used for model validation produce bactericidal effects on both *S. aureus* and *P. aeruginosa* bacteria. The significant reduction in bacteria at 18 hours of the validation samples, compared to control and flat Ti-6Al-4V samples, reinforce the claim that nanotextured surfaces are capable of killing both Gram-negative and Gram-positive bacteria types.

A significant limitation to this model is the experimental design. Ideally, a much larger experimental data set would be used to construct the statistical model (at least 100 experimental conditions with a minimum of 10 measurements taken for each sample). This would allow for a much more accurate model to be formed between the parameter ranges.

Another drawback of the model is that it ignores the fact that the 30 height measurements are taken from 3 samples, treating the data as 30 independent samples. However, this limitation is partially adjusted for by including the sample and replicate number as fixed factors in the univariate regression and general model construction.

Another limitation is that the model is only valid between the tested parameter bounds, i.e. between 0.1 and 1.0 M NaOH, 1 and 10 hours, and 120 and 240°C. As general rule of statistics, the regression model is an attempt to fit initial experimental data. However, if the model is used for a different data set, the fit will not be as good due to statistical fluctuations in the initial data. While the equation may fit the original data quite well (as seen in the experimental validation), extrapolating beyond experimental bounds is tenuous [47].

The model also does not take into account reaction engineering and resulting production rates that occur during the chemical reaction between Ti and NaOH. The statistical model was solely based on physical changes to the substrate, rather than investigating the chemical balance of reactants within

the vessel. To improve the applicability of the model, further investigation into the chemical mechanisms that drive physical growth should be included. Similarly, this work presents the impact of structure height alone on bactericidal behaviour. In reality, bacterial adhesion and antibacterial surface properties are multi-faceted and complex issues. These behaviours depend on several factors such as structure aspect ratio, surface wettability, initial physical attraction to the surface and other physical, biological and chemical processes. It is a combination of these aspects that determines adhesive and cohesive properties of the biofilm.

While the model has some real-world limitations, it is an appropriate and realistic estimate for surface properties, given a specific combination of process variables. The model is applicable for predicting the height of the surface structures in a hydrothermal experiment, where Ti is reacted with NaOH to form TiO<sub>2</sub> structures.

## 5. CONCLUSIONS

This work developed a statistical model based on experimental data to predict the height of TiO<sub>2</sub> structures formed in a hydrothermal reaction between Ti metal and NaOH, as a function of NaOH concentration, reaction time and reaction temperature. Experimental validation showed that the model is accurate, with a 0.5 – 8.5% error margin. Samples used for this validation were also found to have bactericidal effects against *S. aureus* and *P. aeruginosa* bacteria strains. As we move towards an era of antibiotic resistance, optimizing methods such as hydrothermal synthesis for antibacterial surface production will become increasingly important. This predictive model is a useful contribution to the hydrothermal method, and those using it to fabricate nanostructures on metal substrates, as it allowed prediction of structure height before fabrication, increasing process efficiency. The future of this work is to further develop this model to predict bactericidal efficiency of a hydrothermally synthesised surface, given NaOH concentration, reaction time and reaction temperature, as well as to further investigate the role of surface hydrophobicity on bactericidal efficiency.

## 6. DECLARATIONS

**Author Contributions:** AJ performed hydrothermal synthesis, SEM, dimension measurements, bacterial viability tests, statistical analysis and modelling, and wrote main manuscript. PKDVY conceived experiments and modelling concept, supervised and oversaw the whole work, as well as reviewed and approved the final manuscript.

**Funding:** This work was supported by the Queensland University of Technology, through the Research Training Program (RTP) Stipend; and the Australian Research Council (ARC) Discovery Grant [DP180101098].

**Acknowledgments:** The authors would like to thank Dotmar Engineering Plastic Products for providing and sponsoring PFTE, the Central Analytical Research Facility (CARF QUT), Design and Manufacturing Centre (DMC QUT), Institute for Future Environments (IFE QUT) and Institute of Health and Biomedical Innovation (IHBI QUT). The authors would also like to acknowledge the assistance of Professor Zhiyong Li (QUT) and Associate Professor Dimitrios Vagenas to model development.

**Conflicts of Interest:** The authors declare no conflicts of interest.

## 7. REFERENCES

[1] J. Hasan, H.K. Webb, V.K. Truong, S. Pogodin, V.A. Baulin, G.S. Watson, J.A. Watson, R.J. Crawford, E.P. Ivanova, Selective bactericidal activity of nanopatterned superhydrophobic cicada *Psaltoda claripennis* wing surfaces, *Appl. Microbiol. Biotechnol.* 97(20) (2013) 9257-9262.

- [2] S. Pogodin, J. Hasan, V.A. Baulin, H.K. Webb, V.K. Truong, T.H. Phong Nguyen, V. Boshkovikj, C.J. Fluke, G.S. Watson, J.A. Watson, R.J. Crawford, E.P. Ivanova, Biophysical model of bacterial cell interactions with nanopatterned cicada wing surfaces, *Biophys. J.* 104(4) (2013) 835-840.
- [3] C.D. Bandara, S. Singh, I.O. Afara, A. Wolff, T. Tesfamichael, K. Ostrikov, A. Oloyede, Bactericidal effects of natural nanotopography of dragonfly wing on *Escherichia coli*, *ACS Appl. Mater. Interfaces* 9(8) (2017) 6746-6760.
- [4] A. Balčytis, G. Seniutinas, F. Lapierre, S. Juodkakis, Artificial antibacterial surfaces that are simple to fabricate, in: E.P. Ivanova, R.J. Crawford (Eds.), *Antibacterial Surfaces*, Springer International Publishing, Cham, 2015, pp. 27-40.
- [5] H.J. Ensikat, P. Ditsche-Kuru, C. Neinhuis, W. Barthlott, Superhydrophobicity in perfection: The outstanding properties of the lotus leaf, *Beilstein J. Nanotechnol.* 2(1) (2011) 152-161.
- [6] Y.Y. Yan, N. Gao, W. Barthlott, Mimicking natural superhydrophobic surfaces and grasping the wetting process: A review on recent progress in preparing superhydrophobic surfaces, *Adv. Colloid Interface Sci.* 169(2) (2011) 80-105.
- [7] C. Zhang, D.A. McAdams, J.C. Grunlan, Nano/micro-manufacturing of bioinspired materials: A review of methods to mimic natural structures, *Adv. Mater.* 28(30) (2016) 6292-6321.
- [8] T. Diu, N. Faruqi, T. Sjoström, B. Lamarre, H.F. Jenkinson, B. Su, M.G. Ryadnov, Cicada-inspired cell-instructive nanopatterned arrays, *Sci. Rep.* 4 (2014) 7122.
- [9] J. Hasan, K. Chatterjee, Recent advances in engineering topography mediated antibacterial surfaces, *Nanoscale* 7(38) (2015) 15568-15575.
- [10] J. Hasan, R.J. Crawford, E.P. Ivanova, Antibacterial surfaces: The quest for a new generation of biomaterials, *Trends Biotechnol.* 31(5) (2013) 295-304.
- [11] E.P. Ivanova, J. Hasan, H.K. Webb, V.K. Truong, G.S. Watson, J.A. Watson, V.A. Baulin, S. Pogodin, J.Y. Wang, M.J. Tobin, C. Löbbe, R.J. Crawford, Natural bactericidal surfaces: Mechanical rupture of *Pseudomonas aeruginosa* cells by cicada wings, *Small* 8(16) (2012) 2489-2494.
- [12] G. Zhang, J. Zhang, G. Xie, Z. Liu, H. Shao, Cicada wings: A stamp from nature for nanoimprint lithography, *Small* 2(12) (2006) 1440-1443.
- [13] C.M. Bhadra, V.K. Truong, V.T.H. Pham, M. Al Kobaisi, G. Seniutinas, J.Y. Wang, S. Juodkakis, R.J. Crawford, E.P. Ivanova, Antibacterial titanium nano-patterned arrays inspired by dragonfly wings, *Sci. Rep.* 5 (2015) 16817.
- [14] M.N. Dickson, E.I. Liang, L.A. Rodriguez, N. Vollereaux, A.F. Yee, Nanopatterned polymer surfaces with bactericidal properties, *Biointerphases* 10(2) (2015) 021010.
- [15] D.P. Linklater, H.K.D. Nguyen, C.M. Bhadra, S. Juodkakis, E.P. Ivanova, Influence of nanoscale topology on bactericidal efficiency of black silicon surfaces, *Nanotechnology* 28(24) (2017) 9.
- [16] A. Jaggessar, A. Mathew, H. Wang, T. Tesfamichael, C. Yan, P.K.D.V. Yarlagadda, Mechanical, bactericidal and osteogenic behaviours of hydrothermally synthesised TiO<sub>2</sub> nanowire arrays, *J. Mech. Behav. Biomed. Mater.* 80 (2018) 311-319.
- [17] K.X. Zhu, G.X. Hu, Supercritical hydrothermal synthesis of titanium dioxide nanostructures with controlled phase and morphology, *J. Supercrit. Fluids* 94 (2014) 165-173.
- [18] L.E. Fisher, Y. Yang, M.-F. Yuen, W. Zhang, A.H. Nobbs, B. Su, Bactericidal activity of biomimetic diamond nanocone surfaces, *Biointerphases* 11(1) (2016) 011014.
- [19] S.Y. Chou, Nanoimprint lithography, in: S. Cabrini, S. Kawata (Eds.), *Nanofabrication Handbook*, CRC Press, Boca Raton, 2012, pp. 187-206.
- [20] D. Maas, E. Van Veldhoven, P. Chen, V. Sidorkin, H. Salemink, E. Van der Drift, P. Alkemade, Nanofabrication with a helium ion microscope, *Proc. SPIE* 7638(763814) (2010) 763814.
- [21] J. Rodríguez-Hernández, A.L. Cortajarena, *Design of polymeric platforms for selective biorecognition*, 1st ed., Springer International Publishing, Cham, 2015.
- [22] S.H. Emami, R. Salovey, T.E. Hogen-Esch, Peroxide-mediated crosslinking of poly(ethylene oxide), *J. Polym. Sci. A Polym. Chem.* 40(17) (2002) 3021-3026.
- [23] P. Krsko, S. Sukhishvili, M. Mansfield, R. Clancy, M. Libera, Electron-beam surface-patterned poly(ethylene glycol) microhydrogels, *Langmuir* 19(14) (2003) 5618-5625.

- [24] H. Shahali, J. Hasan, A. Mathews, H. Wang, C. Yan, T. Tesfamichael, P.K.D.V. Yarlagadda, Multifunctional properties of three species of cicada wings and biomimetic fabrication of nanopatterned titanium pillars, *Journal of Materials Chemistry B* 7(8) (2019) 1300-1310.
- [25] X.L. Li, Bactericidal mechanism of nanopatterned surfaces, *Phys. Chem. Chem. Phys.* 18(2) (2016) 1311-1316.
- [26] F.D. Xue, J.J. Liu, L.F. Guo, L.R. Zhang, Q.Z. Li, Theoretical study on the bactericidal nature of nanopatterned surfaces, *J. Theor. Biol.* 385 (2015) 1-7.
- [27] A. Velic, T. Tesfamichael, Z. Li, P.K.D.V. Yarlagadda, Parametric Study on Nanopattern Bactericidal Activity, *Procedia Manufacturing* 30 (2019) 514-521.
- [28] J. Hasan, S. Raj, L. Yadav, K. Chatterjee, Engineering a nanostructured "super surface" with superhydrophobic and superkilling properties, *RSC Adv.* 5(56) (2015) 44953-44959.
- [29] N.M. Alves, J. Shi, E. Oramas, J.L. Santos, H. Tomás, J.F. Mano, Bioinspired superhydrophobic poly(L-lactic acid) surfaces control bone marrow derived cells adhesion and proliferation, *J. Biomed. Mater. Res. A* 91(2) (2009) 480-488.
- [30] B.J. Privett, J. Youn, S.A. Hong, J. Lee, J. Han, J.H. Shin, M.H. Schoenfish, Antibacterial fluorinated silica colloid superhydrophobic surfaces, *Langmuir* 27(15) (2011) 9597-9601.
- [31] C. Bhadra, M. Werner, V.A. Baulin, V. Truong, M. Kobaisi, S. Nguyen, A. Balcytis, S. Juodkasis, J. Wang, D. Mainwaring, R. Crawford, E. Ivanova, Subtle Variations in Surface Properties of Black Silicon Surfaces Influence the Degree of Bactericidal Efficiency, *Nano-Micro Letters* 10(2) (2018) 1-8.
- [32] A. Jaggesar, A. Mathew, T. Tesfamichael, H. Wang, C. Yan, P.K. Yarlagadda, Bacteria Death and Osteoblast Metabolic Activity Correlated to Hydrothermally Synthesised TiO<sub>2</sub> Surface Properties, *Molecules* 24(7) (2019) 1201.
- [33] F. Ozel, H. Kockar, O. Karaagac, Growth of iron oxide nanoparticles by hydrothermal process: Effect of reaction parameters on the nanoparticle size, *J Supercond Nov Magn* 28(3) (2015) 823-829.
- [34] X. Chen, S.S. Mao, Titanium dioxide nanomaterials: Synthesis, properties, modifications and applications, *Chem. Rev.* 107(7) (2007) 2891-2959.
- [35] M. Lorenzetti, I. Dogsa, T. Stosicki, D. Stopar, M. Kalin, S. Kobe, S. Novak, The influence of surface modification on bacterial adhesion to Titanium-based substrates, *ACS Appl. Mater. Interfaces* 7(3) (2015) 1644-1651.
- [36] J.-K. Oh, J.-K. Lee, S.J. Kim, K.-W. Park, Synthesis of phase- and shape-controlled TiO<sub>2</sub> nanoparticles via hydrothermal process, *J Ind Eng Chem* 15(2) (2009) 270-274.
- [37] Z. Cui, H. Yang, B. Wang, R. Li, X. Wang, Effect of Experimental Parameters on the Hydrothermal Synthesis of Bi<sub>2</sub>WO<sub>6</sub> Nanostructures, *Nanoscale Research Letters* 11(1) (2016) 190.
- [38] M.D. Wang, C.C. Xing, K. Cao, L. Meng, J.B. Liu, Alignment-controlled hydrothermal growth of well-aligned ZnO nanorod arrays, *J Phys Chem Solids* 75(7) (2014) 808-817.
- [39] B. Liu, E.S. Aydil, Growth of Oriented Single-Crystalline Rutile TiO<sub>2</sub> Nanorods on Transparent Conducting Substrates for Dye-Sensitized Solar Cells, *J. Am. Chem. Soc.* 131(11) (2009) 3985-3990.
- [40] G. Collazzo, S. Jahn, N. Carreño, E. Foletto, Temperature and reaction time effects on the structural properties of titanium dioxide nanopowders obtained via the hydrothermal method, *Braz J Chem Eng* 28(2) (2011) 265-272.
- [41] K. Byrappa, M. Yoshimura, *Handbook of hydrothermal technology*, William Andrew, Norwich, N.Y, 2013.
- [42] M.M. Lencka, R.E. Riman, Synthesis of lead titanate: Thermodynamic modeling and experimental verification, *J. Am. Ceram. Soc.* 76(10) (1993) 2649-2659.
- [43] M.M. Lencka, R.E. Riman, Thermodynamic modeling of hydrothermal synthesis of ceramic powders, *Chem. Mater.* 5(1) (1993) 61-70.
- [44] A. Dias, Theoretical Calculations and Hydrothermal Processing of BaWO<sub>4</sub> Materials Under Environmentally Friendly Conditions, *J Solution Chem* 40(6) (2011) 1126-1139.
- [45] S.-B. Cho, J.-S. Noh, M.M. Lencka, R.E. Riman, Low temperature hydrothermal synthesis and formation mechanisms of lead titanate (PbTiO<sub>3</sub>) particles using tetramethylammonium hydroxide: thermodynamic modelling and experimental verification, *J. Eur. Ceram. Soc.* 23(13) (2003) 2323-2335.

- [46] A. Dias, V.n.S.T. Ciminelli, Thermodynamic calculations and modeling of the hydrothermal synthesis of nickel tungstates, *J. Eur. Ceram. Soc.* 21(10) (2001) 2061-2065.
- [47] G.R. Norman, *PDQ Statistics* (3rd Edition), 3rd ed. ed., B.C. Decker, Hamilton, Ont., 2003.